

Three-dimensional envelope instability model in periodic focusing channels

Ji Qiang*

Lawrence Berkeley National Laboratory, Berkeley, CA 94720, USA

The space-charge driven envelope instability can be of great danger in high intensity accelerators and was studied using a two-dimensional (2D) envelope model and three-dimensional (3D) macroparticle simulations before. In this paper, we propose a three-dimensional envelope instability model to study the instability for a bunched beam in a periodic solenoid and radio-frequency (RF) focusing channel and a periodic quadrupole and RF focusing channel. This study shows that when the transverse zero current phase advance is below 90 degrees, the beam envelope can still become unstable if the longitudinal zero current phase advance is beyond 90 degrees. For the transverse zero current phase advance beyond 90 degrees, the instability stopband width becomes larger with the increase of the longitudinal focusing strength and even shows different structure from the 2D case when the longitudinal zero current phase advance is beyond 90 degrees. Breaking the symmetry of two longitudinal focusing RF cavities and the symmetry between the horizontal focusing and the vertical focusing in the transverse plane in the periodic quadrupole and RF channel makes the instability stopband broader. This suggests that a more symmetric accelerator lattice design might help reduce the range of the envelope instability in parameter space.

I. INTRODUCTION

The envelope instability as a space-charge driven collective instability presents a potentially great danger in high intensity accelerators by causing beam size blow up and quality degradation. It has been studied theoretically [1–8] and experimentally [9–11] since 1980s. In recent years, there was growing interest in further understanding this instability and other structural resonances [12–22]. Some of those studies were summarized in a recently published monograph [23]. However, most of those theoretical studies were based on a two-dimensional model. Three-dimensional macroparticle simulations were carried out for a bunched beam under the guidance of the two-dimensional envelope instability model [16, 19]. It was found in reference [16] that the instability stopband from the 3D macroparticle simulation is broader than that from the 2D envelope model. Furthermore, the effect of the longitudinal synchrotron motion has not been systematically studied in those macroparticle simulations and is missed in the 2D envelope instability model. In this paper, we proposed a three-dimensional envelope instability model in periodic focusing channels. Such a model can be used to systematically study the effect of longitudinal synchrotron motion on the instability stopband for a bunched beam. It can also be used to explore the stability in a fully 3D parameter space and to provide guidance for 3D macroparticle simulations.

The organization of this paper is as follows: after the introduction, we review the 2D envelope instability model in Section II; we present the 3D envelope instability model in Section III; we present numerical study of the envelope instability in a periodic transverse solenoid and longitudinal RF focusing channel in Section IV; we present numerical study of the envelope instability in a periodic transverse quadrupole and longitudinal RF focusing channel in Section V; and draw conclusions in Section VI.

II. TWO-DIMENSIONAL ENVELOPE INSTABILITY MODEL

For a two-dimensional coasting beam subject to external periodic focusing forces and linear space-charge forces, the two-dimensional envelope equations are given as[2, 24]:

$$\frac{d^2 X}{ds^2} + k_x^2(s)X - \frac{K/2}{X+Y} - \frac{\epsilon_x^2}{X^3} = 0 \quad (1)$$

$$\frac{d^2 Y}{ds^2} + k_y^2(s)Y - \frac{K/2}{X+Y} - \frac{\epsilon_y^2}{Y^3} = 0 \quad (2)$$

*Electronic address: jqiang@lbl.gov

where X and Y are horizontal and vertical rms beam sizes respectively, k_x^2 and k_y^2 represent the external periodic focusing forces, ϵ_x and ϵ_y denote unnormalized rms emittances, and K is the generalized perveance associated with the space-charge strength given by:

$$K = \frac{qI}{2\pi\epsilon_0 p_0 v_0^2 \gamma_0^2} \quad (3)$$

where I is the current of the beam, q is the charge of the particle, ϵ_0 is the vacuum permittivity, p_0 is the momentum of the reference particle, v_0 is the speed of the reference particle, and γ_0 is the relativistic factor of the reference particle.

The above equations can be linearized with respect to a periodic solution (i.e. matched solution) as:

$$X(s) = X_0(s) + x(s) \quad (4)$$

$$Y(s) = Y_0(s) + y(s) \quad (5)$$

where X_0 and Y_0 denote the periodic matched envelope solutions and x and y denote small perturbations

$$x(s) \ll X_0(s), \quad y(s) \ll Y_0(s) \quad (6)$$

The equations of motion for the small perturbations are given by:

$$\frac{d^2 x(s)}{ds^2} + a_1(s)x(s) + a_{12}(s)y(s) = 0 \quad (7)$$

$$\frac{d^2 y(s)}{ds^2} + a_2(s)y(s) + a_{12}(s)x(s) = 0 \quad (8)$$

where

$$a_{12}(s) = 2K/(X_0(s) + Y_0(s))^2 \quad (9)$$

$$a_1(s) = k_x^2(s) + 3\epsilon_x^2/X_0^4(s) + a_{12}(s) \quad (10)$$

$$a_2(s) = k_y^2(s) + 3\epsilon_y^2/Y_0^4(s) + a_{12}(s) \quad (11)$$

With $\xi = (x, x', y, y')^T$, the prime denotes derivative with respect to s , and T denotes the transpose of a matrix, the above equations can be rewritten in matrix notation as:

$$\frac{d\xi}{ds} = A_4(s)\xi(s) \quad (12)$$

with the periodic matrix

$$A_4(s) = \begin{pmatrix} 0 & 1 & 0 & 0 \\ -a_1(s) & 0 & -a_{12}(s) & 0 \\ 0 & 0 & 0 & 1 \\ -a_{12}(s) & 0 & -a_2(s) & 0 \end{pmatrix} \quad (13)$$

Let $\xi(s) = M_4(s)\xi(0)$ be the solution of above equation, substituting this equation into Eq. 12 results in

$$\frac{dM_4(s)}{ds} = A_4(s)M_4(s) \quad (14)$$

where $M_4(s)$ denotes the 4×4 transfer matrix solution of $\xi(s)$ and $M_4(0)$ is a 4×4 unit matrix. The matrix $A_4(s)$ is a periodic function of s with a length of period L . Following the Floquet's theorem, the solution of $M_4(s)$ after n lattice periods can be written as

$$M_4(s + nL) = M_4(s)M_4(L)^n \quad (15)$$

This matrix solution will remain finite as $n \rightarrow \infty$, only if all amplitudes of the eigenvalues of the matrix $M_4(L)$ be less than or equal to one. Since the matrix $M_4(L)$ is a real symplectic matrix, the eigenvalues of the matrix occur both as reciprocal and as complex-conjugate pairs. Therefore, for stable solutions, all eigenvalues of the matrix $M_4(L)$ have to lie on a unit circle in the complex plane. The eigenvalues of the matrix $M_4(L)$ can be expressed in polar coordinates as:

$$\lambda = |\lambda| \exp(i\phi) \quad (16)$$

where the amplitude $|\lambda|$ of the eigenvalue gives the growth rate (or damping rate) of the envelope eigenmode through one lattice period and the phase shift ϕ of the eigenvalue gives the phase of the envelope mode oscillation through one period. For an unstable envelope mode, there are two possibilities [2]:

1. one or both eigenvalue pairs lie on the real axis: $\phi_{1,2} = 180^\circ$,
2. the phase shift angles are equal: $\phi_1 = \phi_2$.

The first case can be seen as a half-integer parametric resonance between the focusing lattice and the envelope oscillation mode. The second case is a confluent resonance between two envelope oscillation modes since they have the same oscillation frequencies.

III. THREE-DIMENSIONAL ENVELOPE INSTABILITY MODEL

The 3D envelope equations have been used to study the halo particle formation mechanism (e.g. particle-core model) for a bunched beam in high intensity accelerators [25–28]. There, the mismatched envelope oscillation resonates with a test particle and drives the particle into large amplitude becoming a halo particle. The mismatched envelope oscillation itself is stable in that case. In this paper, we study the stability/instability of the mismatched envelope oscillation itself in periodic focusing channels.

For a 3D uniform density ellipsoidal beam inside a periodic focusing channel without acceleration, the three-dimensional envelope equations are given as [29, 30]:

$$\frac{d^2 X}{ds^2} + k_x^2(s)X - I_x(X, Y, Z)X - \frac{\epsilon_x^2}{X^3} = 0 \quad (17)$$

$$\frac{d^2 Y}{ds^2} + k_y^2(s)Y - I_y(X, Y, Z)Y - \frac{\epsilon_y^2}{Y^3} = 0 \quad (18)$$

$$\frac{d^2 Z}{ds^2} + k_z^2(s)Z - I_z(X, Y, Z)Z - \frac{(\epsilon_z/\gamma^2)^2}{Z^3} = 0 \quad (19)$$

with

$$I_i(X, Y, Z) = C \int_0^\infty \frac{dt}{(e_i^2 + t)\sqrt{(X^2 + t)(Y^2 + t)(\gamma^2 Z^2 + t)}} \quad (20)$$

where X , Y , and Z are horizontal, vertical, and longitudinal rms beam sizes respectively, $e_i = X, Y, \gamma Z$, for $i = x, y, z$, and $C = \frac{1}{2} \frac{3}{4\pi\epsilon_0} \frac{q}{mc^2} \frac{I}{f_{rf}\beta^2\gamma^2} \frac{1}{5\sqrt{5}}$. Here, ϵ_0 is the vacuum permittivity, q the charge, mc^2 the rest energy of the particle, c the light speed in vacuum, I the average beam current, f_{rf} the RF bunch frequency, $\beta = v/c$, v the bunch velocity, and the relativistic factor $\gamma = 1/\sqrt{1 - \beta^2}$.

The above equations can be linearized with respect to periodic solutions (i.e. matched solutions) as:

$$X(s) = X_0(s) + x(s) \quad (21)$$

$$Y(s) = Y_0(s) + y(s) \quad (22)$$

$$Z(s) = Z_0(s) + z(s) \quad (23)$$

where X_0 , Y_0 and Z_0 denote the periodic matched envelope solutions and x , y and z denote small perturbations

$$x(s) \ll X_0(s), \quad y(s) \ll Y_0(s), \quad z(s) \ll Z_0(s) \quad (24)$$

The equations of motion for these small perturbations are given by:

$$\frac{d^2 x}{ds^2} + a_1(s)x(s) + a_{12}(s)y(s) + \gamma^2 a_{13}(s)z(s) = 0 \quad (25)$$

$$\frac{d^2 y}{ds^2} + a_{12}(s)x(s) + a_2(s)y(s) + \gamma^2 a_{23}(s)z(s) = 0 \quad (26)$$

$$\frac{d^2 z}{ds^2} + a_{13}(s)x(s) + a_{23}(s)y(s) + a_3(s)z(s) = 0 \quad (27)$$

where

$$a_1(s) = k_x^2 + 3\epsilon_x^2/X_0^4 - I_x(X_0, Y_0, Z_0) + 3X_0^2 F_{xx} \quad (28)$$

$$a_{12}(s) = X_0 Y_0 F_{xy} \quad (29)$$

$$a_{13}(s) = X_0 Z_0 F_{xz} \quad (30)$$

$$a_2(s) = k_y^2 + 3\epsilon_y^2/Y_0^4 - I_y(X_0, Y_0, Z_0) + 3Y_0^2 F_{yy} \quad (31)$$

$$a_{23}(s) = Y_0 Z_0 F_{yz} \quad (32)$$

$$a_3(s) = k_z^2 + 3(\epsilon_z/\gamma^2)^2/Z_0^4 - I_z(X_0, Y_0, Z_0) + 3\gamma^2 Z_0^2 F_{zz} \quad (33)$$

where

$$F_{xx} = C \int_0^\infty (X_0^2 + t)^{-5/2} (Y_0^2 + t)^{-1/2} (Z_0^2 \gamma^2 + t)^{-1/2} dt \quad (34)$$

$$F_{xy} = C \int_0^\infty (X_0^2 + t)^{-3/2} (Y_0^2 + t)^{-3/2} (Z_0^2 \gamma^2 + t)^{-1/2} dt \quad (35)$$

$$F_{xz} = C \int_0^\infty (X_0^2 + t)^{-3/2} (Y_0^2 + t)^{-1/2} (Z_0^2 \gamma^2 + t)^{-3/2} dt \quad (36)$$

$$F_{yy} = C \int_0^\infty (X_0^2 + t)^{-1/2} (Y_0^2 + t)^{-5/2} (Z_0^2 \gamma^2 + t)^{-1/2} dt \quad (37)$$

$$F_{yz} = C \int_0^\infty (X_0^2 + t)^{-1/2} (Y_0^2 + t)^{-3/2} (Z_0^2 \gamma^2 + t)^{-3/2} dt \quad (38)$$

$$F_{zz} = C \int_0^\infty (X_0^2 + t)^{-1/2} (Y_0^2 + t)^{-1/2} (Z_0^2 \gamma^2 + t)^{-5/2} dt \quad (39)$$

With $\xi = (x, x', y, y', z, z')^T$, the above equations can be rewritten in matrix notation as:

$$\frac{d\xi}{ds} = A_6(s)\xi(s) \quad (40)$$

with the periodic matrix

$$A_6(s) = \begin{pmatrix} 0 & 1 & 0 & 0 & 0 & 0 \\ -a_1(s) & 0 & -a_{12}(s) & 0 & -\gamma^2 a_{13}(s) & 0 \\ 0 & 0 & 0 & 1 & 0 & 0 \\ -a_{12}(s) & 0 & -a_2(s) & 0 & -\gamma^2 a_{23}(s) & 0 \\ 0 & 0 & 0 & 0 & 0 & 1 \\ -a_{13}(s) & 0 & -a_{23}(s) & 0 & -a_3(s) & 0 \end{pmatrix} \quad (41)$$

Let $\xi(s) = M_6(s)\xi(0)$, substituting this equation into Eq. 40 results in

$$\frac{dM_6(s)}{ds} = A_6(s)M_6(s) \quad (42)$$

where $M_6(s)$ denotes the 6×6 transfer matrix solution of $\xi(s)$ and $M_6(0)$ is a 6×6 unit matrix. The above ordinary differential equation can be solved using the matched envelope solutions and numerical integration. Similar to the 2D envelope instability model, the stability of these envelope perturbations is determined by the eigenvalues of the transfer matrix $M_6(L)$ through one lattice period. For the envelope oscillation to be stable, all eigenvalues of the $M_6(L)$ have to stay on the unit circle. The amplitude of the eigenvalue gives the envelope mode growth (or damping) rate through one lattice period, while the phase of the eigenvalue yields the mode oscillation frequency. When the amplitude of any eigenvalue is greater than one, the envelope oscillation becomes unstable.

IV. ENVELOPE INSTABILITY IN A PERIODIC SOLENOID AND RF CHANNEL

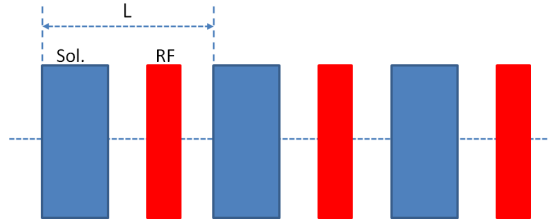


FIG. 1: Schematic plot of a periodic solenoid and RF channel.

We first studied the envelope instability in a transverse solenoid focusing and longitudinal RF focusing periodic channel. A schematic plot of this periodic channel is shown in Fig. 1. Each period of the channel consists of a

0.2 meter solenoid and a 0.1 meter RF bunching cavity. The total length of the period is 0.5 meters. The proton bunch has a kinetic energy of 150 MeV and normalized rms emittances of 0.2 μm , 0.2 μm , and 0.2 μm in horizontal, vertical, and longitudinal directions respectively. Figures 2-3 show the 3D envelope mode amplitudes and phases as a function of transverse depressed phase advance for different zero current transverse and longitudinal phase advances. As a comparison, we also show in Figs. 4-5 the 2D envelope mode amplitudes and phases as a function of depressed transverse phase advance for the same zero current transverse phase advances. Here, the 2D periodic solenoid channel has the same length of period as the 3D channel. It is seen that in the 2D periodic solenoid channel, the envelope instability occurs when the zero current phase advance is over 90 degrees. In the 3D periodic solenoid-RF channel, the envelope instability occurs even with the zero current transverse phase advance 80 degrees but longitudinal phase advance beyond 90 degrees as shown in Fig. 2 (a2). There is no instability if both the transverse zero current phase advance and the longitudinal zero current phase advance are below 90 degrees as seen in Fig. 2 (a1). For the 3D envelope modes, when the longitudinal zero current phase advance below 90 degrees and the transverse zero current phase above 90 degrees as shown in Figs 2 (b1, c1, and d1), the instability stopband becomes broader as the zero current longitudinal phase advance increases. This is probably because the longitudinal synchrotron motion helps bring particles with different depressed transverse tunes into the resonance. A faster synchrotron motion might result in more particles falling into the resonance and hence a broader instability stopband. For small longitudinal zero current phase advance (e.g. 20 degrees), the 3D envelope mode show the stopband similar to that of the 2D envelope mode. When the longitudinal zero current phase advance is above 90 degrees, as shown in Fig. 2 (b2, c2, and d2), the 3D envelope instability shows more complicated structure and larger instability stopband width than the 2D envelope instability.

In the 2D periodic transverse solenoid focusing channel, for a coasting beam with equal horizontal and vertical emittances, it is seen in Fig. 5, the envelope instabilities are due to the 180 degree half-integer parametric resonance. However, for a bunched beam, as shown in Fig. 3, besides the 180 degree half-integer resonance, there are also confluent resonances where two envelope modes have the same frequencies and resonate with each other. The existence of both instability mechanisms results in more complicated structure as shown in Figs. 2 (b2, c2, and d2).

The 3D envelope instability shows asymmetry between the transverse direction and the longitudinal direction in the 3D periodic solenoid and RF channel. Figure 6 shows the envelope mode phases as a function of depressed transverse phase advance for a case with zero current 80 degree transverse phase advance and 120 degree longitudinal phase advance, and a case with zero current 120 degree transverse phase advance and 80 degree longitudinal phase advance. The envelope mode amplitudes for both cases are shown in Fig. 2 (a2 and c1). For the 80 degree zero current transverse phase advance, there is only one major unstable stopband below 30 degree depressed transverse phase advance due to half-integer parametric resonance as shown in the left plot of Fig. 6. For the 120 degree zero current transverse phase advance, there are three unstable regions, two due to the half-integer parameter resonance and one due to the confluent resonance as shown in the right plot of Fig. 6. This asymmetry is probably related to the two degrees of freedom in the transverse plane while only one in the longitudinal direction.

V. ENVELOPE INSTABILITY IN A PERIODIC QUADRUPOLE-RF CHANNEL

Next, we studied the 3D envelope instability in a periodic transverse quadrupole focusing and longitudinal RF focusing channel for the same bunched proton beam. A schematic plot of this periodic channel is shown in Fig. 7. Each period of the channel consists of a 0.2 meter focusing quadrupole, a 0.1 meter RF focusing cavity, a 0.2 meter defocusing quadrupole and another 0.1 meter RF bunching cavity. The total length of the period is 1.0 meters. Figures 8-9 show the 3D envelope mode amplitudes and phases as a function of transverse depressed phase advance for different zero current transverse and longitudinal phase advances. As a comparison, we also show in Figs 10-11 the 2D envelope mode amplitudes and phases as a function of the depressed phase advance for different zero current phase advances. Here, the 2D periodic quadrupole channel has the same length of period as the 3D channel. It is seen that in the 2D periodic quadrupole channel, the envelope instability occurs when the zero current phase advance is over 90 degrees. There is no instability when the zero current phase advance is below 90 degrees. In the 3D periodic quadrupole-RF channel, the envelope instability occurs even with the zero current transverse phase advance 80 degrees but the longitudinal phase advance beyond 100 degrees in Fig. 8 (a2). There is no instability if both the transverse zero current phase advance and the longitudinal zero current phase advance are below 90 degrees. For the 3D envelope modes, when the longitudinal zero current phase advance is below 90 degrees and the transverse zero current phase above 90 degrees as shown in Fig. 8 (b1, c1, and d1), the instability stopband width increases with the increase of the zero current longitudinal phase advance. For small longitudinal zero current phase advance (e.g. 20 degrees), the 3D envelope modes instability stopband is similar to that of the 2D envelope modes. For the 100 degree zero current transverse phase advance case, when the zero current longitudinal phase advance is beyond 90 degrees, the stopband becomes more complicated and shows multiple stopbands. For the transverse zero current 120

and 140 degree phase advances, the instability stopbands do not change significantly with the increase of zero current longitudinal phase advance. This is probably due to the fact that when the transverse zero current phase advance is beyond 100 degrees, most parameter space (transverse depressed tune) below 90 degrees becomes unstable caused by the confluent resonance. Further increasing the zero current longitudinal phase advance beyond 90 degrees will not enlarge that stopband any more.

In the periodic transverse quadrupole focusing channel, it is seen in Fig. 11, the 2D envelope instabilities are mainly due to the confluent resonance between the two envelope modes when their phases become equal. This appears still to be valid in the 3D periodic quadrupole-RF channel as shown in Fig. 9.

The 3D envelope instability shows asymmetry between the transverse and the longitudinal direction in the 3D periodic quadrupole and RF channel too. Figure 12 shows the envelope mode phases as a function of depressed transverse phase advance for a case with zero current 80 degree transverse phase advance and 120 degree longitudinal phase advance, and a case with zero current 120 degree transverse phase advance and 80 degree longitudinal phase advance. The envelope mode amplitudes are shown in Fig. 8 (a2 and c1) for this comparison. For the 80 degree zero current transverse phase advance, there is only one major unstable region around 60 degree depressed transverse phase advance due to the confluent resonance. For the 120 degree zero current phase advance, there are two unstable regions due to two confluent resonances.

In the above periodic quadrupole and RF channel, we assumed that the two RF cavities have the same longitudinal focusing strength. The longitudinal focusing period is half of the transverse focusing period. This accounts for the absence of the envelope instability for the zero current 80 degree transverse phase advance and 100 degree longitudinal phase in the periodic quadrupole and RF channel. The envelope instability stopband is observed in the periodic solenoid and RF channel with the same zero current phase advances as shown in Fig. 2 (a2). The absence of instability for longitudinal zero current phase advance 100 degrees was also observed in 3D macroparticle simulations in reference [22]. Now, we break the symmetry of two RF longitudinal focusing cavities, the longitudinal focusing period becomes the same as the transverse focusing period. The envelope instability occurs for these zero current phase advances in a periodic quadrupole and RF channel. Figures 13 show the envelope mode amplitudes and phases as a function of transverse depressed phase advances with about 10%, 20%, and 30% deviation from the original setting of the two RF cavities (one cavity plus that percentage and the other one minus that percentage). It is seen that as the asymmetry between the two RF cavity increases, the instability stopband width also increases. Before breaking of the symmetry of two RF cavities, the longitudinal phase advance per longitudinal period is 50 degrees. After the breaking of the symmetry, the longitudinal period becomes the same as the lattice period and the phase advance becomes 100 degrees. Such a zero current phase advance results in half integer parametric resonance as shown in Fig. 13.

In above 3D periodic solenoid/quadrupole and RF transport channels, we have assumed that in transverse plane, the zero current phase advances in horizontal direction and the vertical direction are the same. Furthermore, the bunch has the same emittances in both horizontal and vertical directions. This might imply a two-dimensional transverse and longitudinal periodic system (i.e. $r-z$). As a comparison, we also calculated the envelope mode amplitudes and phases for a true two-dimensional periodic quadrupole channel with different zero current phase advances in the horizontal and the vertical direction (120 degrees in the horizontal direction and 80 degrees in the vertical direction). Figure 14 shows the 2D envelope mode amplitudes and phases as a function of the depressed horizontal and vertical phase advance. Comparing the 2D envelope mode amplitudes and phases in above plot with those of the 3D envelope mode with the same zero current phase advances in Figs. 2 (a2) and 8 (a2) (80 degrees in transverse and 120 in longitudinal) and Fig. 2 (c1) and 8 (c1) (120 degrees in transverse and 80 in longitudinal), we see that the 2D envelope instability shows somewhat similar structure to the 3D envelope instability in a periodic solenoid-RF channel with transverse zero current phase advance 80 degrees and longitudinal phase advance 120 degrees. The major instabilities in both cases are caused by the half-integer parametric resonance. The 3D envelope modes in a periodic quadrupole-RF channel shows quite different instability stopband from the 2D envelope modes. Also the 3D envelope instability in quadrupole channel is caused by the confluent resonance while the 2D asymmetric envelope instability in the quadrupole channel is mainly caused by the half-integer parametric resonance.

We also explored 3D envelope instabilities with non-equal transverse zero current phase advances in the horizontal direction and the vertical direction. Figure 15 shows the 3D envelope mode amplitudes and phases as a function of the depressed horizontal tune with zero current phase advance 120 degrees in the horizontal direction, 110 degrees in the vertical direction, and 80 degrees in the longitudinal direction in the periodic quadrupole and RF channel. Comparing the above figure with the zero current 120 degree transverse phase advance and 80 degree longitudinal phase advance case in Fig. 8 (c1), we see that 3D instability stopband from the nonequal transverse focusing becomes broader. Instead of one major instability stopband and a minor stopband in the equal transverse phase advance case, now there are four stopbands (two major stopbands and two minor stopbands) for the transverse 120 and 110 degree phase advances. Besides the confluent resonance, there also appears a half-integer parametric resonance when the transverse symmetry is broken. Breaking the transverse symmetry results in more resonances of these envelope modes.

This suggests that keeping the same zero current phase advance in both the horizontal and the vertical directions might help reduce the parameter region of the envelope instability.

VI. CONCLUSIONS

In this paper, we proposed a three-dimensional envelope instability model to study the instability for a bunched beam in a periodic solenoid and RF focusing channel and a periodic quadrupole and RF focusing channel. This study showed that when the transverse zero current phase advance is below 90 degrees, the beam envelope can still become unstable if the longitudinal zero current phase advance is beyond 90 degrees. For the transverse zero current phase advance beyond 90 degrees, the instability stopband becomes broader with the increase of longitudinal focusing strength and even shows different structure from the 2D case when the longitudinal zero current phase advance is beyond 90 degrees.

The 3D envelope instability shows asymmetry between the longitudinal focusing and the transverse focusing. The instability shows broader stopband when the transverse zero current phase advance is beyond 90 degrees than that when the longitudinal zero current phase advance is beyond 90 degrees. In the 3D periodic quadrupole and RF channel, for the transverse zero current phase advance 80 degree, the envelope modes stay stable for the longitudinal 100 degree zero current phase advance due to the symmetry of two longitudinal focusing RF cavities. Breaking the symmetry of two cavities results in the envelope instability with a finite stopband. Breaking the horizontal and vertical focusing symmetry in the transverse plane also increases the envelope instability stopband width. This suggests that a more symmetric accelerator lattice design might help reduce the parameter space of the envelope instability.

ACKNOWLEDGEMENTS

Work supported by the U.S. Department of Energy under Contract No. DE-AC02-05CH11231. We would like to thank Dr. R. D. Ryne for the use of his 2D and 3D envelope codes. This research used computer resources at the National Energy Research Scientific Computing Center.

-
- [1] I. Hofmann, L. J. Laslett, L. Smith, and I. Haber, *Part. Accel.* 13, 145 (1983).
 - [2] J. Struckmeier and M. Reiser, *Part. Accel.* 14, 227 (1984).
 - [3] I. Hofmann, *Phys. Rev. E* 57, 4713 (1998).
 - [4] R. C. Davidson, H. Qin, and G. Shvets, *Phys. Plasmas* 7, 1020 (2000).
 - [5] H. Okamoto and K. Yokoya, *Nucl. Instrum. Methods Phys. Res., A* 482, 51 (2002).
 - [6] A. V. Fedotov and I. Hofmann, *Phys. Rev. Spec. Top.-Accel. Beams* 5, 024202 (2002).
 - [7] A. V. Fedotov, I. Hofmann, R. L. Gluckstern, and H. Okamoto, *Phys. Rev. Spec. Top.-Accel. Beams* 6, 094201 (2003).
 - [8] S. M. Lund and B. Bukh, *Phys. Rev. Spec. Top.-Accel. Beams* 7, 024801 (2004).
 - [9] M. Tiefenback, "Space charge limits on the transport of ion beams in a long alternating gradient system," Ph.D. thesis, Lawrence Berkeley National Laboratory Report LBL-22465, 1986.
 - [10] E. P. Gilson, M. Chung, R. C. Davidson P. C. Efthimion, and R. Majeski, *Phys. Rev. Spec. Top.-Accel. Beams* 10, 124201 (2007).
 - [11] L. Groening, W. Barth, W. Bayer, G. Clemente, L. Dahl, P. Forck, P. Gerhard, I. Hofmann, M. S. Kaiser, M. Maier, S. Mickat, and T. Milosic, *Phys. Rev. Lett.* 102, 234801 (2009).
 - [12] D. Jeon, L. Groening, and G. Franchetti, *Phys. Rev. Spec. Top.-Accel. Beams* 12, 054204 (2009).
 - [13] K. Fukushima, K. Itoa, H. Okamoto, S. Yamaguchi, K. Moriya, H. Higaki, T. Okano, and S. M. Lund, *Nucl. Instrum. Methods Phys. Res., A* 733, 18 (2014).
 - [14] C. Li and Y. L. Zhao, *Phys. Rev. ST Accel. Beams* 17, 124202 (2014).
 - [15] C. Li and Q. Qin, *Phys. Plasmas* 22, 023108 (2015).
 - [16] I. Hofmann and O. Boine-Frankenheim, *Phys. Rev. Lett.* 115, 204802 (2015).
 - [17] D. Jeon, J. H. Jang, and H. Jin, *Nucl. Instrum. Methods Phys. Res., A* 832, 43 (2016).
 - [18] O. Boine-Frankenheim, I. Hofmann, and J. Struckmeier, *Phys. Plasmas* 23, 090705 (2016).
 - [19] I. Hofmann and O. Boine-Frankenheim, *Phys. Rev. Accel. Beams* 20, 014202 (2017).
 - [20] K. Ito, H. Okamoto, Y. Tokashiki, and K. Fukushima, *Phys. Rev. Accel. Beams* 20, 064201 (2017).
 - [21] Y. Yuan, O. Boine-Frankenheim, and I. Hofmann, *Phys. Rev. Accel. Beams* 20, 104201 (2017).
 - [22] I. Hofmann and O. Boine-Frankenheim, *Phys. Rev. Lett.* 118, 114803, (2017).
 - [23] I. Hofmann, "Space Charge Physics for Particle Accelerators," Springer, 2017.
 - [24] I. Kapchinskiy and V. Vladimirov, 2nd Conf. High Energy Accel., p. 274, CERN, Geneva, 1959.
 - [25] K. Bongardt, M. Pabst and A. Letchford, in *Proc. 1998 Linac Conf.*, p. 824, 1999.

- [26] C. Allen, in Proc. of the 2nd ICFA Advanced Accelerator Workshop, Ed. J. Rosenzweig and L. Serafini, p. 173, World Scientific, 2000.
- [27] J. Qiang and R. D. Ryne, Phys. Rev. ST Accel. Beams 3, 064201 (2000).
- [28] M. Comunian, A. Pisent, A. Bazzani, G. Turchetti, and S. Rambaldi, Phys. Rev. ST Accel. Beams 4, 124201 (2001).
- [29] F. J. Sacherer, IEEE Trans. Nucl. Sci. 18, 1101 (1971).
- [30] R. Ryne, Los Alamos Report No. LA-UR-95-391;; <http://xxx.lanl.gov/abs/acc-phys/9502001>.

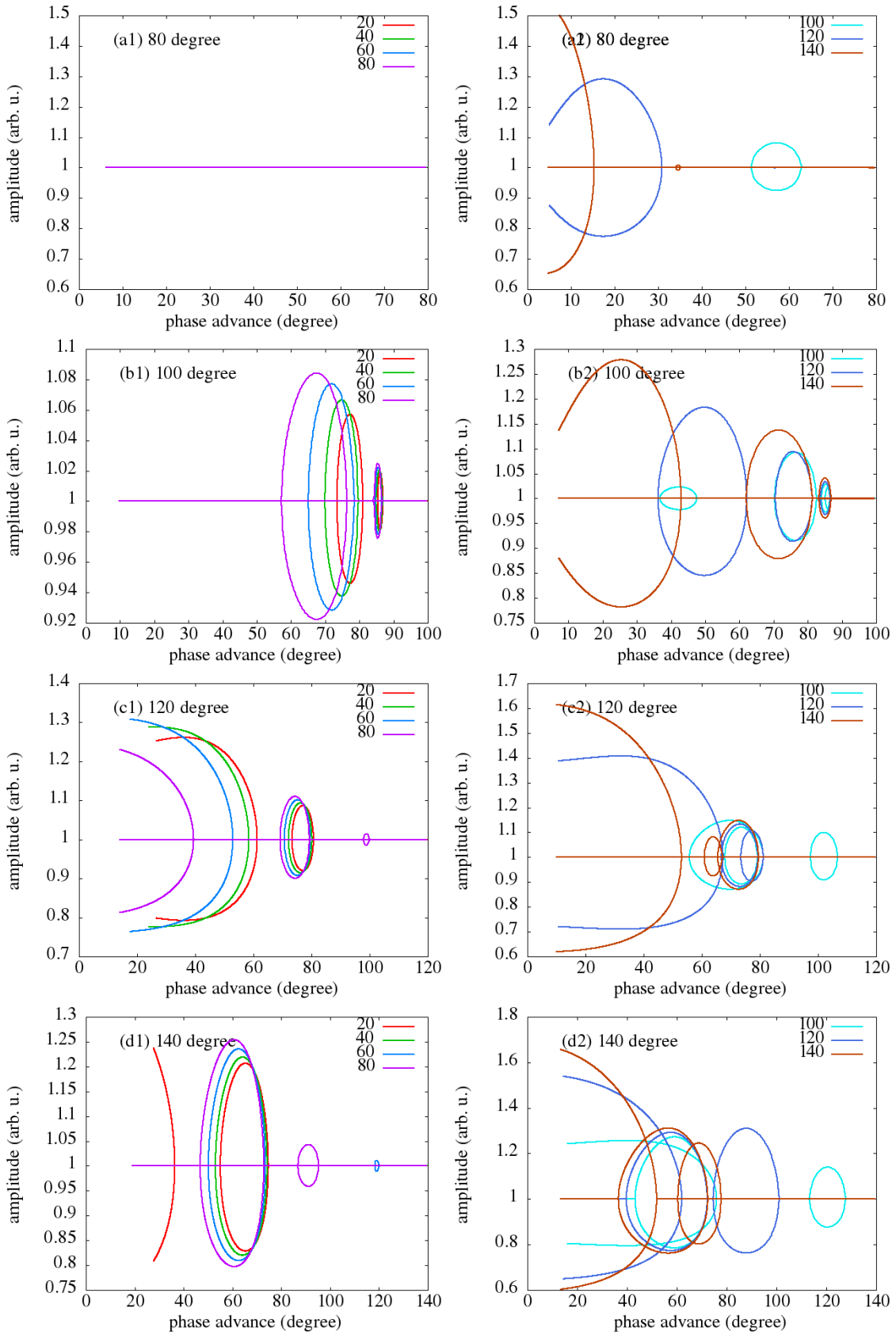


FIG. 2: The 3D envelope mode amplitudes as a function of depressed transverse phase advance with 20, 40, 60, 80, 100, 120, and 140 degree zero current longitudinal phase advances for (a) 80 degree, (b) 100 degree, (c) 120 degree, and (d) 140 degree zero current transverse phase advances in a periodic solenoid-RF channel.

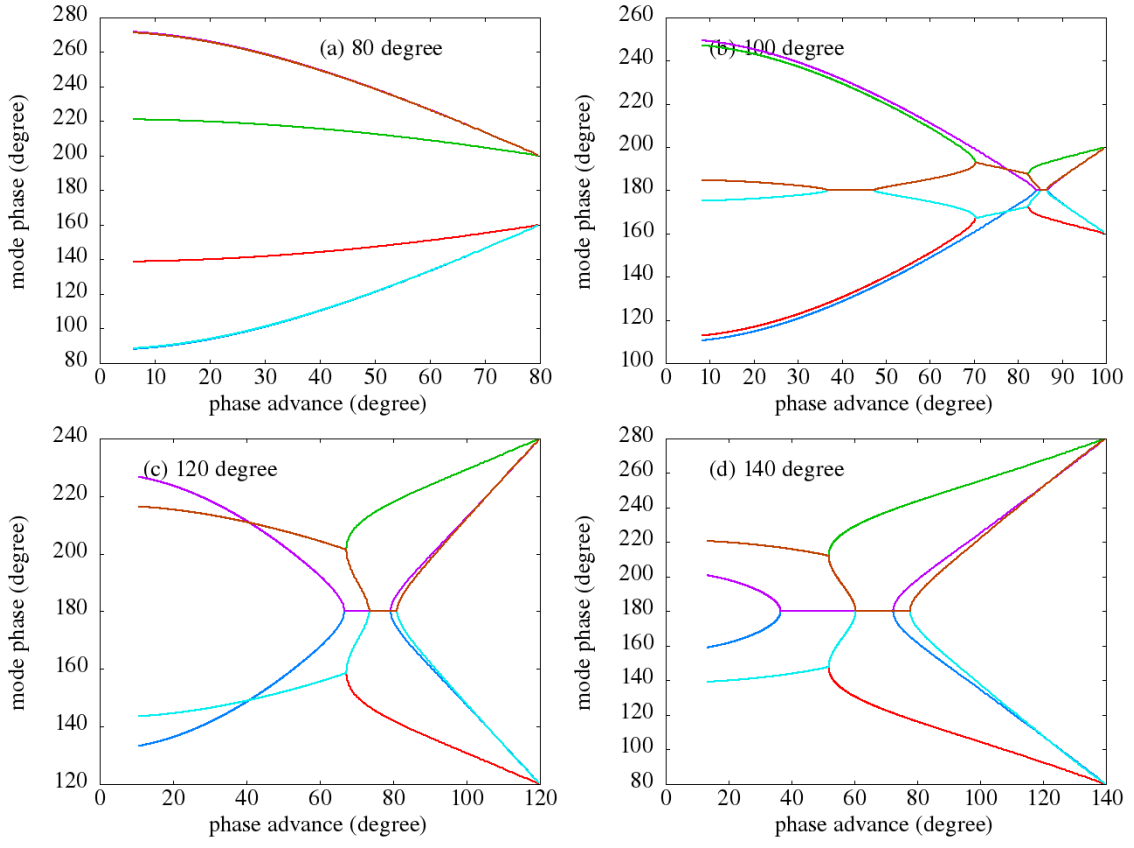


FIG. 3: The 3D envelope mode phases as a function of depressed transverse phase advance with (a) 80 degree, (b) 100 degree, (c) 120 degree, and (d) 140 degree zero current longitudinal and transverse phase advances in a periodic solenoid-RF channel.

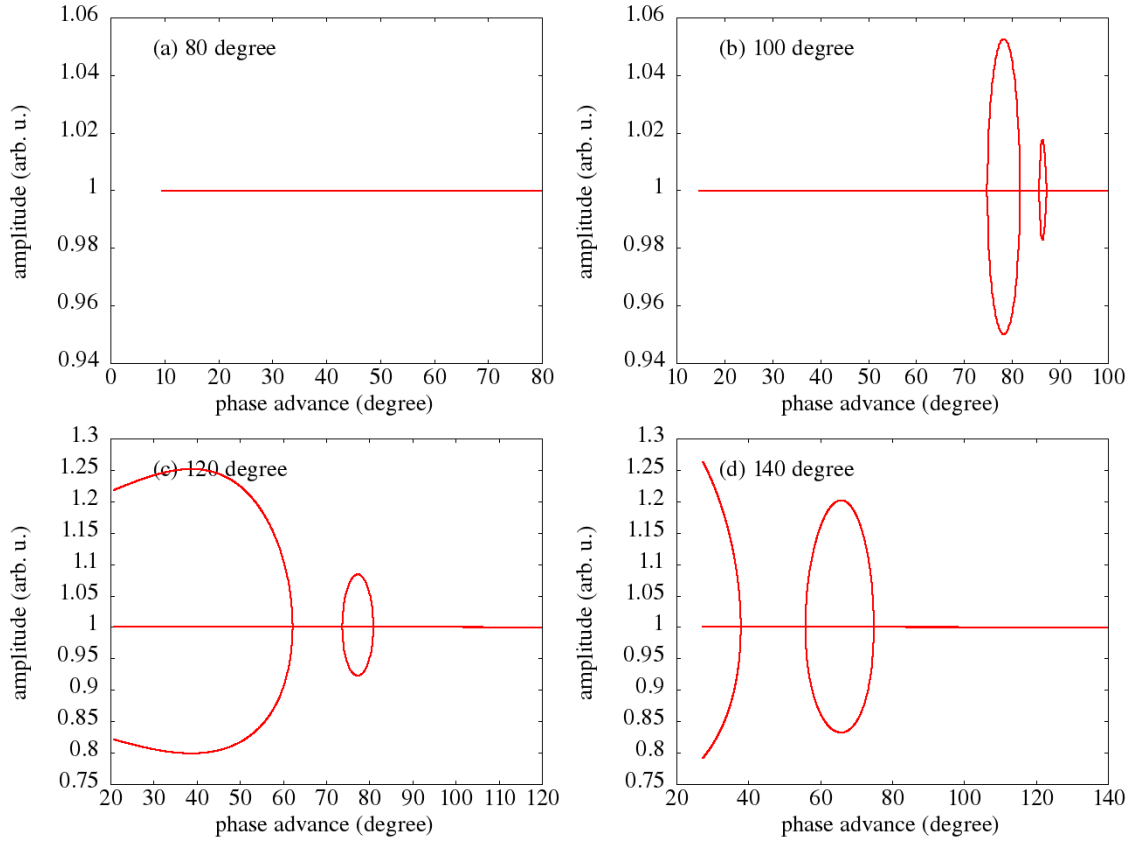


FIG. 4: The 2D envelope mode amplitudes as a function of depressed transverse phase advance for (a) 80 degree, (b) 100 degree, (c) 120 degree, and (d) 140 degree zero current transverse phase advances in a periodic solenoid channel.

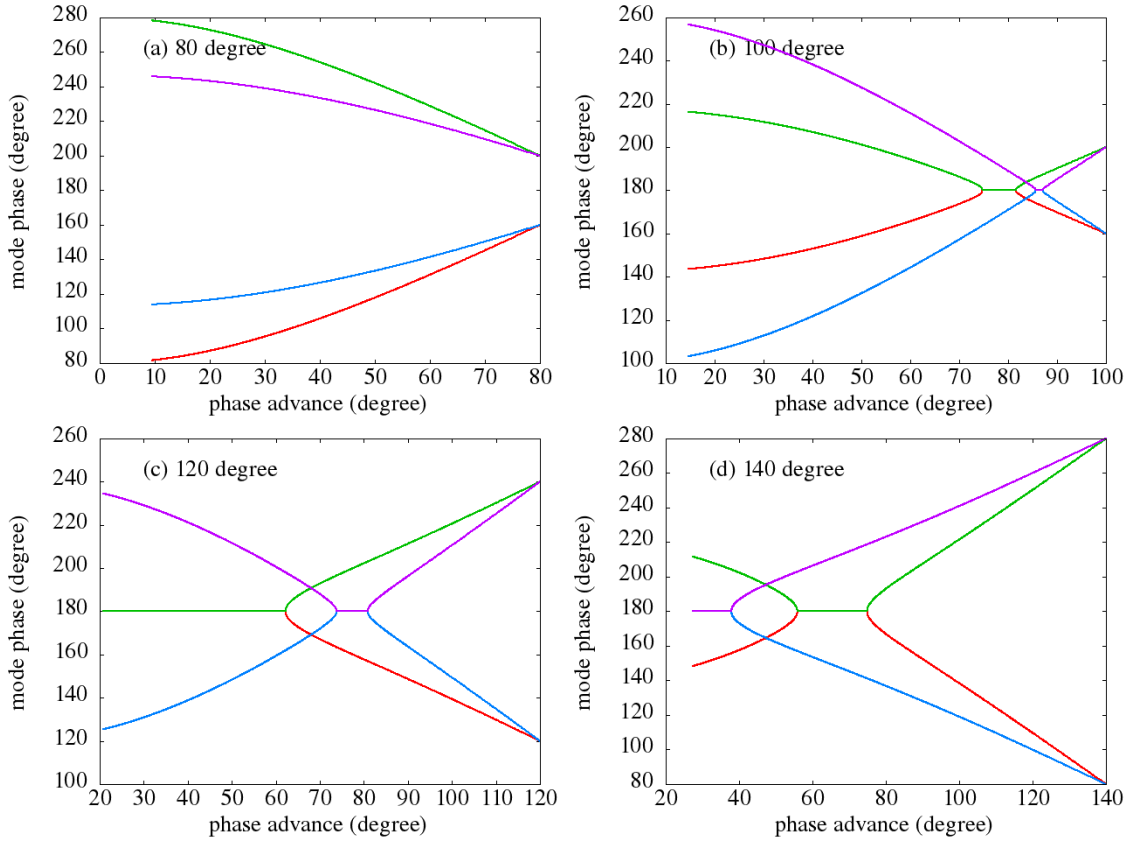


FIG. 5: The 2D envelope mode phases as a function of depressed transverse phase advance for (a) 80 degree, (b) 100 degree, (c) 120 degree, and (d) 140 degree zero current transverse phase advances in a periodic solenoid channel.

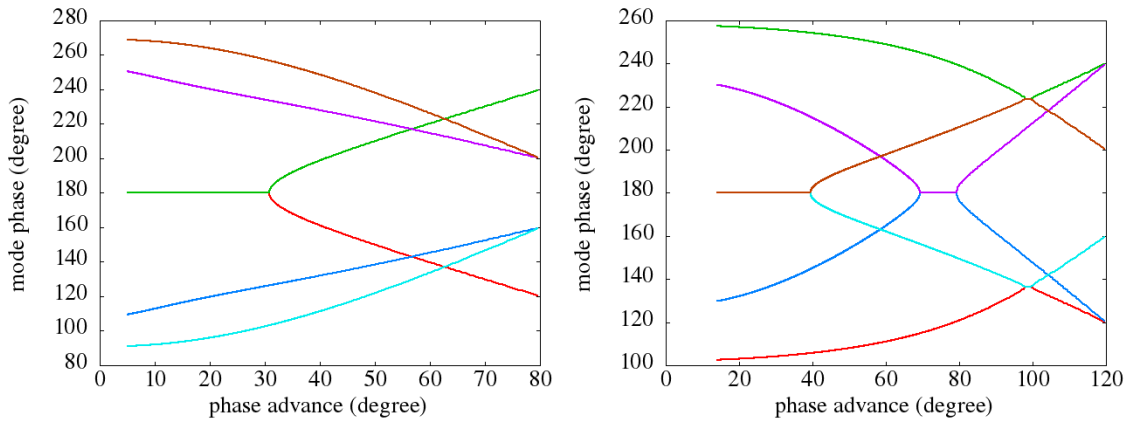


FIG. 6: The 3D envelope mode phases as a function of the depressed transverse phase advance for zero current (a) transverse 80 degree and longitudinal 120 degree, (b) transverse 120 degree and longitudinal 80 degree phase advance in a periodic solenoid channel.

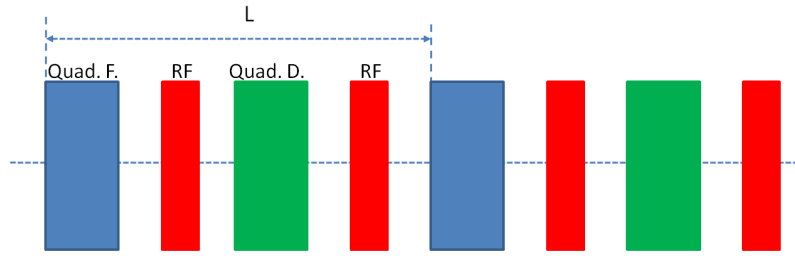


FIG. 7: Schematic plot of a periodic quadrupole and RF channel.

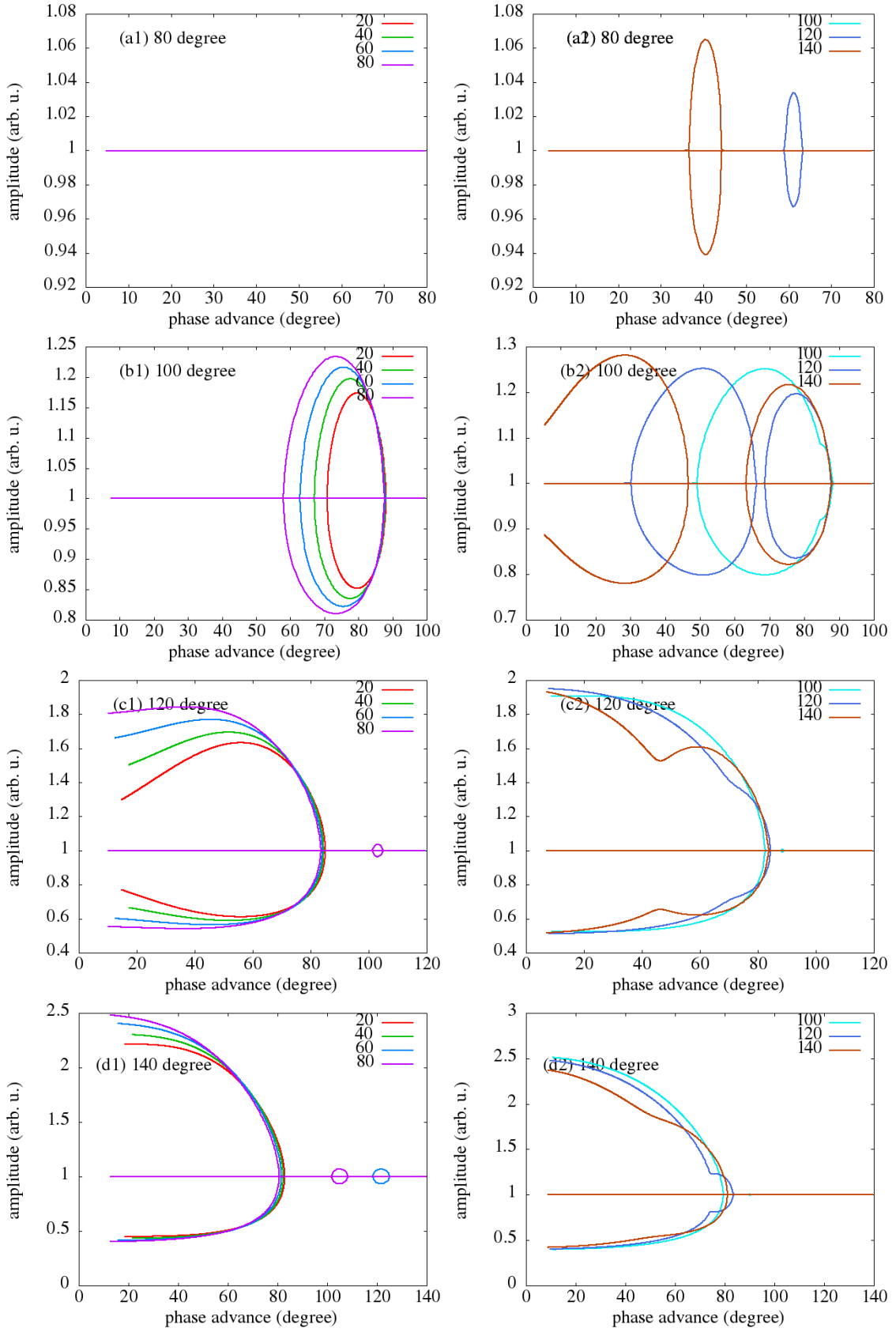


FIG. 8: The 3D envelope mode amplitudes as a function of depressed transverse phase advance with 20, 40, 60, 80, 100, 120, and 140 degree zero current longitudinal phase advances for (a) 80 degree, (b) 100 degree, (c) 120 degree, and (d) 140 degree zero current transverse phase advances in a periodic quadrupole-RF channel.

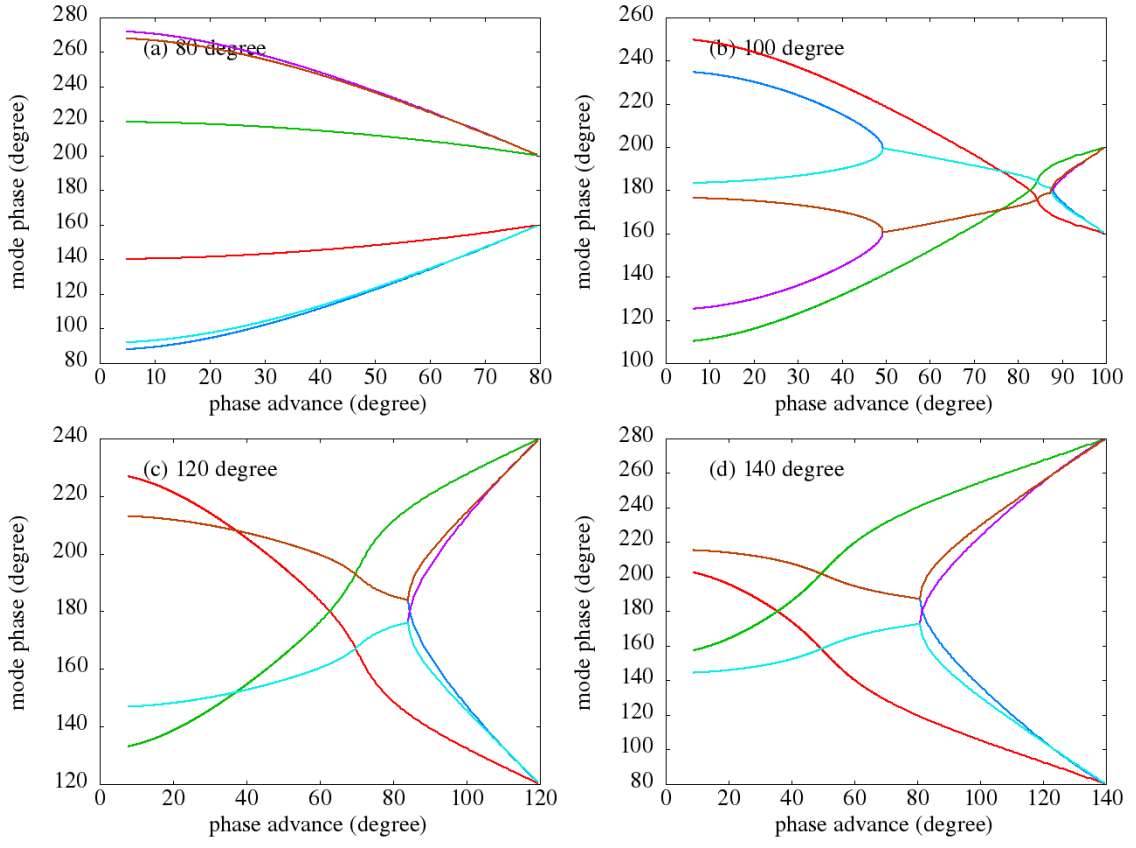


FIG. 9: The 3D envelope mode phases as a function of depressed transverse phase advance with (a) 80 degree, (b) 100 degree, (c) 120 degree, and (d) 140 degree zero current longitudinal and transverse phase advances in a periodic quadrupole-RF channel.

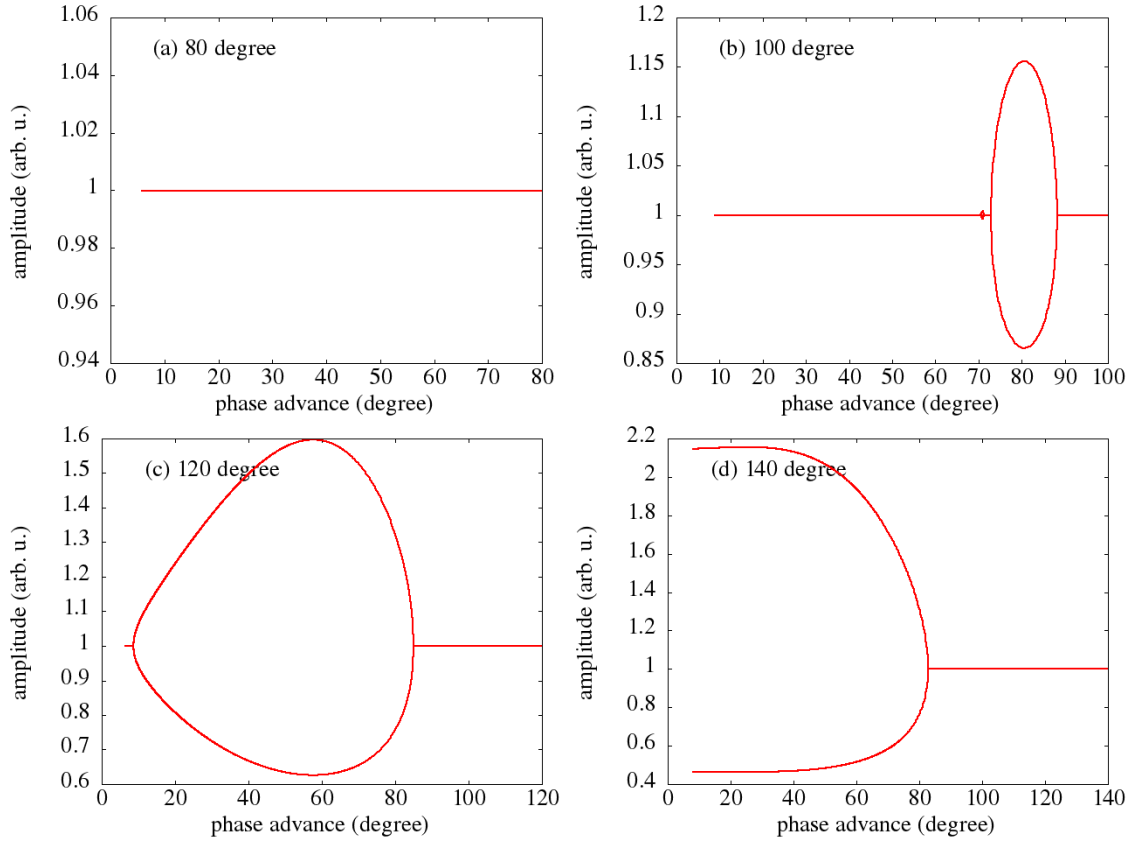


FIG. 10: The 2D envelope mode amplitudes as a function of depressed transverse phase advance for (a) 80 degree, (b) 100 degree, (c) 120 degree, and (d) 140 degree zero current transverse phase advances in a periodic quadrupole channel.

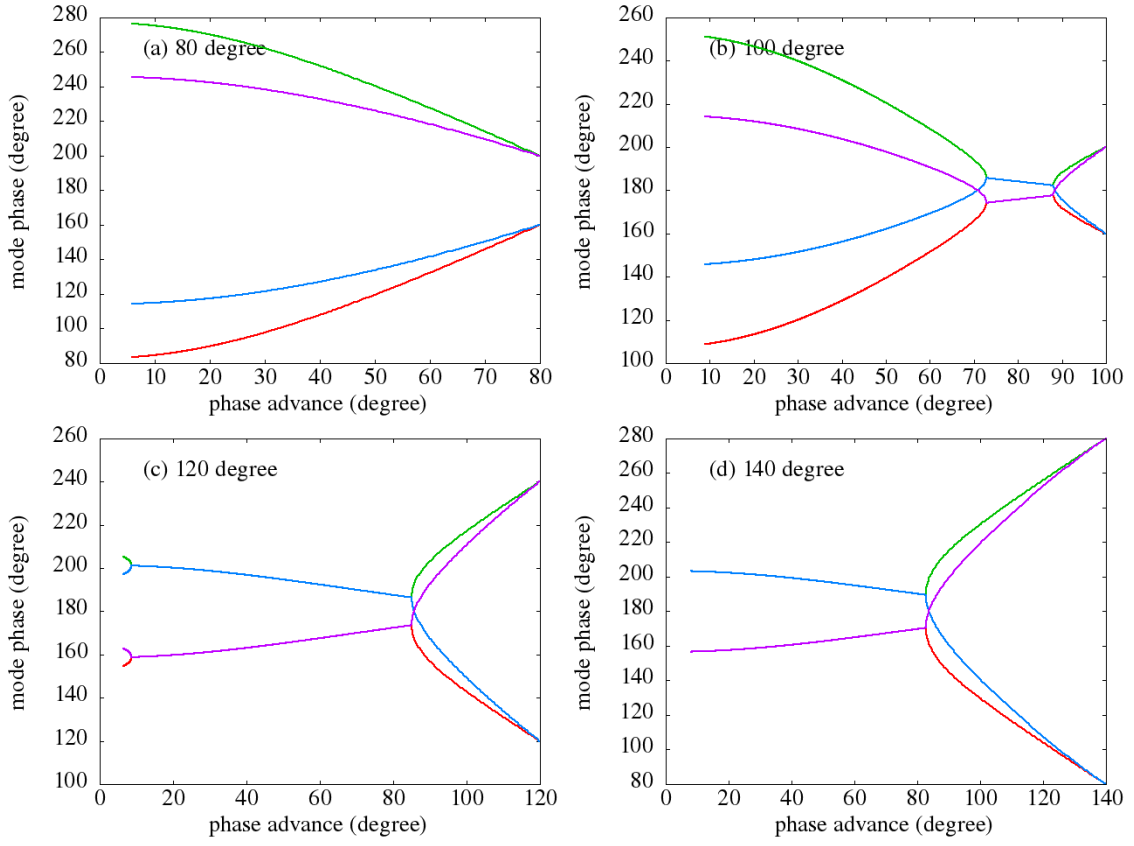


FIG. 11: The 2D envelope mode phases as a function of depressed transverse phase advance for (a) 80 degree, (b) 100 degree, (c) 120 degree, and (d) 140 degree zero current transverse phase advances in a periodic quadrupole channel.

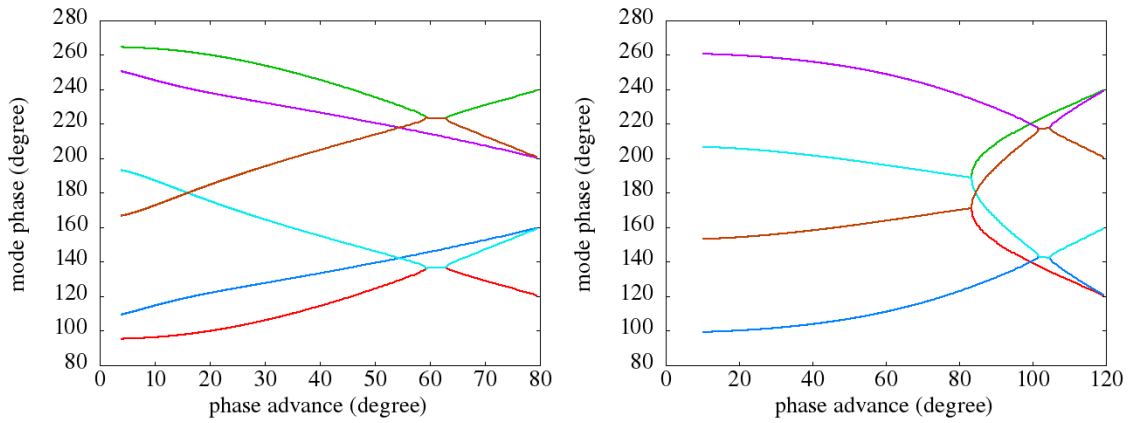


FIG. 12: The 3D envelope mode phases as a function of depressed transverse phase advance for zero current (a) transverse 80 degree and longitudinal 120 degree, (b) transverse 120 degree and longitudinal 80 degree phase advance in a periodic quadrupole channel.

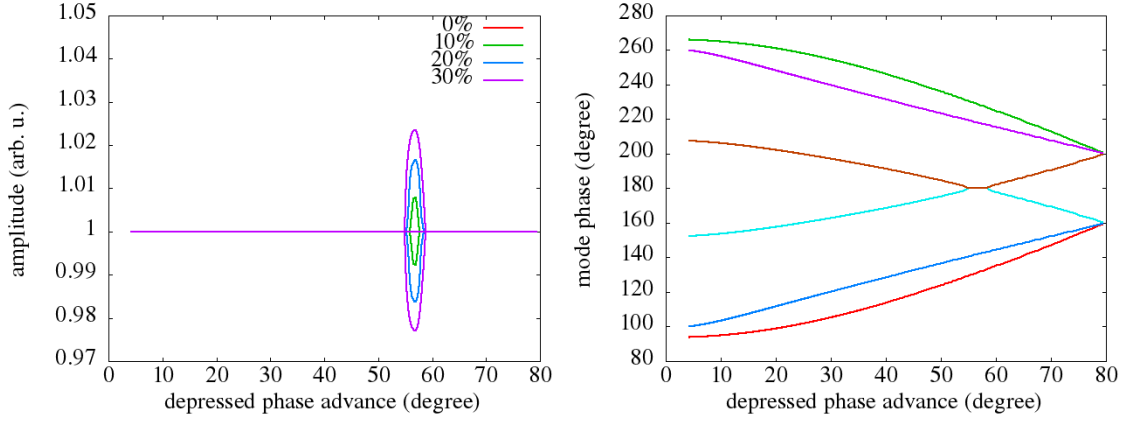


FIG. 13: The 3D envelope mode (left) amplitudes and (right) phases as a function of the transverse depressed phase advance with 10%, 20%, and 30% deviations from the original RF cavity setting in a periodic quadrupole-RF channel.

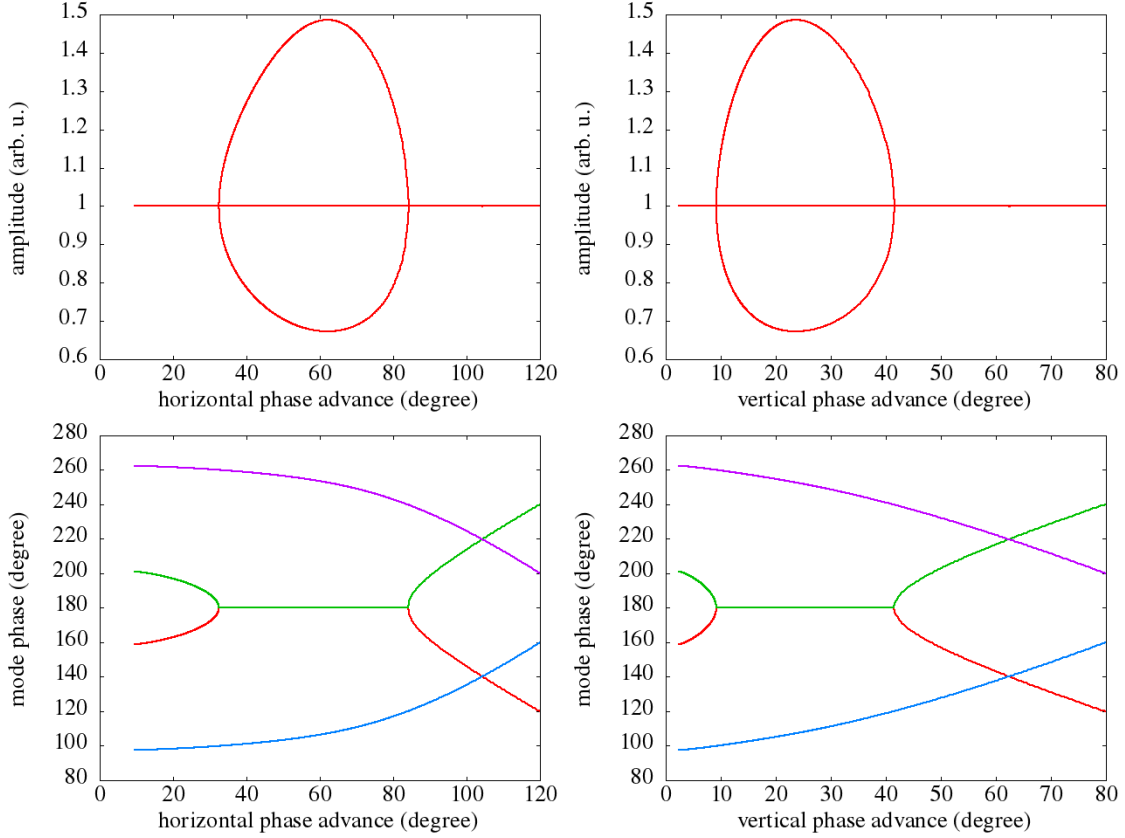


FIG. 14: The 2D envelope mode (top) amplitudes and (bottom) phases as a function of depressed phase advance with asymmetric zero current phase advances (80 degrees in one direction and 120 degrees in another direction) in a periodic quadrupole channel.

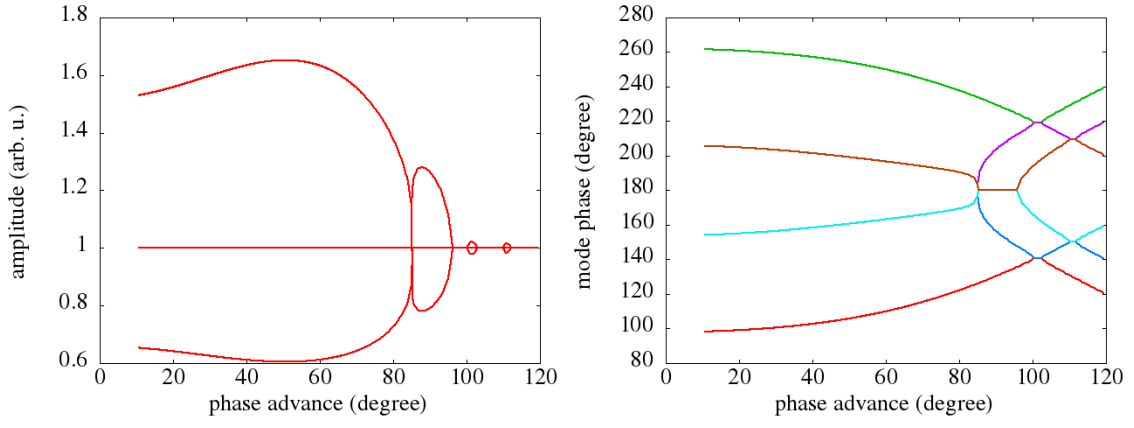


FIG. 15: The 3D envelope mode (left) amplitudes and (right) phases as a function of the horizontal depressed phase advances with zero current phase advances 120 degrees in horizontal, 110 in vertical, and 80 in longitudinal direction in a periodic quadrupole-RF channel.